Climate Dynamics (2001) 17: 527–546

F. Vauclair · Y. du Penhoat

Interannual variability of the upper layer of the tropical Atlantic Ocean from in situ data between 1979 and 1999

Received: 18 April 2000 / Accepted: 20 July 2000

Abstract Interannual variability of the upper layers of the tropical Atlantic is described based on in situ data. An objective analysis used all available temperature observations of the upper tropical Atlantic between 1979 and 1999 to construct a 4D database. Wind data are used to investigate potential mechanisms which might explain the observed variability. Four remarkable events are described: 1983–1984, 1988–1990, 1994–1995 and 1997–1998. Three of them are characterised as equatorial (1983–1984, 1994–1995, and 1997–1998). The 1988–1990 event is a basin-wide phenomenon which does not involve the same mechanisms as the other three. Results of statistical decomposition in empirical orthogonal functions (EOFs) are discussed. There is no evidence of an inter-hemispheric mode on the depth of the 20 °C-isotherm (D20) and heat content comparable to the observed mode for sea surface temperature (SST) fields. Most energetic patterns for D20 and heat content are dominated by the stronger variability in the northern part of the basin. Influences of other climate signals are investigated. Correlations between the winter NAO (North Atlantic Oscillation) index and our standard variables is marginally significant. A positive NAOW (North Atlantic Oscillation of Winter) is associated with SST cooling in a latitude band between 10°N and 20°N. When applied to the El-Niño index, correlations are much more significant. We found two scales of maximum correlation: at the four month lag after the El-Niño mature phase when the thermocline slope and zonal heat content gradient are maximum along the equator, and at the ten month lag after the mature phase of El-Niño when the thermocline slope weakens and the equatorial gradient of heat content vanished. The correlation with a zonal wind index (average between 30°W–35°W and 2°N–2°S) has been computed. Correlation is maximum at the six month lag when the thermocline slope and the zonal heat content gradient are maximum in the equatorial band. This ''Atlantic Niño'' mode is influenced by the Pacific Ocean's variability and reaches a maximum one year after a warm event in the eastern Pacific.

F. Vauclair (✉) · Y. du Penhoat
LEGOS-GRGS, 18 Av. Edouard Belin,
31401, Toulouse Cedex 4, France
E-mail: Fabrice.vauclair@cnes.fr

1 Introduction

The tropical Atlantic Ocean has a great influence on the surrounding continents. Unlike the Pacific Ocean in which the interannual ENSO (El-Niño Southern Oscillation) signal dominates the variability of the upper ocean, the tropical Atlantic is characterised by a large seasonal cycle. This seasonal cycle is very strongly visible down to thermocline waters, while it is much less significant in the lower part, below the thermocline (Merle 1980). This predominant seasonal signal is visible at the depth of the 20 °C isotherm (D20), which is a proxy for the thermocline depth in the tropics, as well as for the heat content integrated over the upper 400 m. In spite of this strong seasonal cycle, climatically significant interannual to decadal time scales deviations are observed. Significant economic and scientific interests justify studies which may lead to better knowledge and understanding of the climatic variability in these areas, in order to predict the evolution of specific climatic parameters. Until the beginning of the 1980s, the number of subsurface temperature observations was not sufficient to investigate the interannual temperature variability of the whole tropical Atlantic basin. Most previous works dealt only with sea surface temperature (SST) due to the lack of subsurface data over a long period.

The seasonal cycle of the tropical Atlantic has been well documented (Merle et al. 1980; Servain 1986 among others). It is mainly caused by the meridional excursion of the Inter-Tropical Convergence Zone (ITCZ) which reaches its northernmost position in July–September and its southernmost position in January–March when it is close to the equator (Merle 1980). Its annual signal is

characterised by a large SST amplitude (2° to 4°) near the equator with significant spatial variations. An intensification of this amplitude is noted south of the equator (0° to 4°S) in the Gulf of Guinea. It rapidly decreases with depth down to the thermocline.

Superimposed on the mean seasonal cycle of the SST, two main modes of interannual variability can be distinguished using statistics: a meridional mode, which has no counterpart in the Pacific, characterised by the variability of the inter-hemispheric gradient of SST, and an equatorial mode analogous to, but weaker than, the Pacific ENSO mode (Servain et al. 1999b). These modes have significant effects on the climate of the surrounding continents. The inter-hemispheric mode reflects the meridional fluctuations of the ITCZ position. In particular, a north-south anomaly of SST gradient is associated with a northward displacement of the ITCZ which causes drought in the Nordeste region of Brazil and more rains in the Sahel. Conversely, a south–north anomaly of the SST gradient, associated with a southward displacement of the ITCZ induces strong rains in Nordeste and drought in the Sahel (Moura and Shukla 1981; Servain 1991; Nobre and Shukla 1996). Furthermore, the variability of upper layer temperature in the northern part of the basin affects rainfall in the Caribbean and modulates cyclone activity (Shaeffer 1995). Whether the gradient mode results from an actual dipole mode in SST distribution or whether the north and south SST variability are unrelated is still an open question. Is it a physical feature or a statistical artifact? Houghton and Tourre (1992) and Mehta and Delworth (1995) claimed a statistical independence between northern and southern regions. On the other hand, Servain (1991), and Nobre and Shukla (1996), among others, support the dipolar structure which fluctuates on a decadal time scale.

The second mode revealed by statistical analysis is the "ENSO like" equatorial mode (e.g. Merle et al. 1980). This shows an interannual variability over a period of a few years. During the warm phase, trade winds are weaker in the western part of the basin, the equatorial SST is higher than normal mainly in the eastern part (Gulf of Guinea). During the cold phase, the trade winds in the western part are stronger and the SST at the equator is colder. The impact of this mode on the climate appears to be very significant, mainly for countries around the Gulf of Guinea (Fontaine et al. 1999) and for northeastern Brazil. The influence on local ecosystems and consequently on fishing are important (Wagner and da Silva 1994). Servain et al. (1999) have recently highlighted a possible relation between these two modes.

The influence of the Pacific ENSO on Atlantic variability has been identified in some studies (Zebiak 1993; Enfield and Mayer 1997). A weak Southern Oscillation Index (SOI) associated with a warm event in the Pacific, would reinforce the westward winds in the Atlantic and vice versa. This could trigger thermocline zonal slope variability in the Atlantic with a lag of a few months (Delecluse et al. 1994). However, correlations (even lagged-correlations) between the equatorial Atlantic mode and El-Niño are weak. Enfield and Mayer (1997), on the basis of observations, establish a connection between warming to the north of the equator in the Atlantic and the mature phase of El-Niño in the Pacific. According to these authors, the warm phase in the Pacific (low SOI: normalised pressure difference between Tahiti and Darwin, and high NINO3 index: mean Pacific SST between 150°W–90°W and 5°N–5°S) is associated with a reinforcement of the high-pressure system in the southern subtropical Atlantic and a weakened high-pressure system in the northern subtropical Atlantic. This means that a Pacific El-Niño event is followed in the tropical Atlantic by a reinforcement of the southeast trade winds and a weakening of the northeast trade winds which lead to warming of the northern tropical basin and cooling of the southern tropical basin. Warming in the northern tropical Atlantic appears to follow a warm phase in the Pacific with a 4 to 5 month lag.

SST variability is driven mainly by three factors: air-sea heat fluxes, upper layer advection and subsurface dynamics. In order to understand the influence of the tropical Atlantic Ocean on climate, subsurface variability has to be investigated. Most of the previous studies on modes of variability were based on surface data. We have investigated subsurface variability of the tropical Atlantic Ocean using all available temperature observations made from 1979 to 1999. We have described the subsurface interannual variability of temperature using an index, D20, which is a proxy for the depth of the thermocline in most of the tropical Atlantic, and heat content, in order to find to what extent subsurface and surface variability are linked.

In Sect. 2, we describe the data and method used to obtain the gridded fields. In Sect. 3, the seasonal cycle and interannual signal are analysed. Four remarkable events of the last 20 years are also examined and finally results of an analysis using empirical orthogonal functions of the surface temperature, D20 and heat content are discussed. In Sect. 4, remote connections between tropical Atlantic and tropical Pacific interannual variability are investigated. Section 5 contains a discussion of our results, a summary and conclusion.

2 Data and method

We collected all available near surface and subsurface observations of the tropical Atlantic between 1979 and 1999 in order to build a gridded data set of surface and subsurface temperatures (TAOSTA : Tropical Atlantic Ocean Subsurface Temperature Atlas). These data come from various sources: XBT (TOGA/WOCE subsurface DATA centre), CTD and Nansen casts from oceanographic cruises, moorings in 1983–1984, and PALACE floats (Profiling Autonomous Lagrangian circulation Experiment) in 1998–1999. The data from PIRATA (Pilot Research Moored Array in the Tropical Atlantic) moorings are also inclued for the last two years . We thus have compiled approximately 120 000 profiles which do not have a uniform distribution. Figure 1 shows the total number of profiles per month summed over the whole basin, and the

non-homogeneity of the temporal coverage of the data. Figure 2 illustrates the distribution of the data. The best sampled areas are along commercial lines and there is little sampling south of 10°S in the central Atlantic.

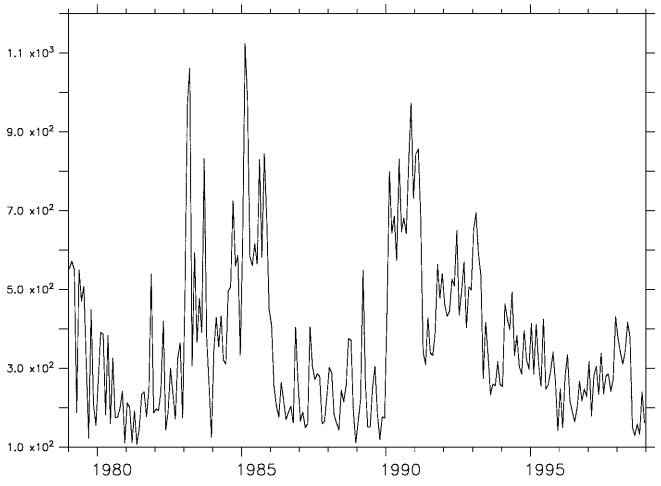

Fig. 1 Number of profiles per month used for the objective analysis. Summed for the whole basin: 70°W–12°E, 30°S–30°N

We interpolated the profiles on the standard Levitus levels. Anomalies were computed using Mayer et al. (1998) monthly climatology, interpolated at the place of measurement. Based on the Bretherton et al. (1976) technique, an optimal interpolation method was used (see e.g. De-Mey and Benkiran 2000), taking into account the spatial and temporal scales of the involved physics. We chose a correlation radius of 800 km in longitude, 300 km in latitude and 31 days in time. The correlation function used was $f(r,t) = (1 + a * r + 1/3 * (a * r)^2) * \exp(-a * r) * \exp(-t^2)$ where $a = 2.10380$ which presents no negative lobe. The optimal interpolation scheme solves a local problem at each grid point using the neighbouring data only (suboptimal mode). This technique is commonly used in numerical weather forecasting, (see e.g. Gustavsson 1981; Lorenc 1986). Suboptimal parameters used to define the influence bubble were 1500 km for the longitude radius, 700 km for the latitude radius and 63 days for the temporal radius. Data were weighted according to their expected accuracy estimated from the data source and the accuracy of the measurement techniques (Table 1). For example, more weight was given to WOCE CTD measurements which are the most precise data.

The domain of analysis extends from 70°W to 12°E and 30°S to 30°N, with 2° latitude-longitude mesh. Vertical profiles are interpolated on Levitus standard levels (from surface to 500 m). The temporal resolution is two months in order to get enough observations at each time step (120 time steps centred on January 30 for January–February, March 30 for March–April ...).

After analysis, we reconstructed the total signal and computed an average seasonal cycle. This was required because the climatology used for a first guess (Mayer et al. 1998), which was based

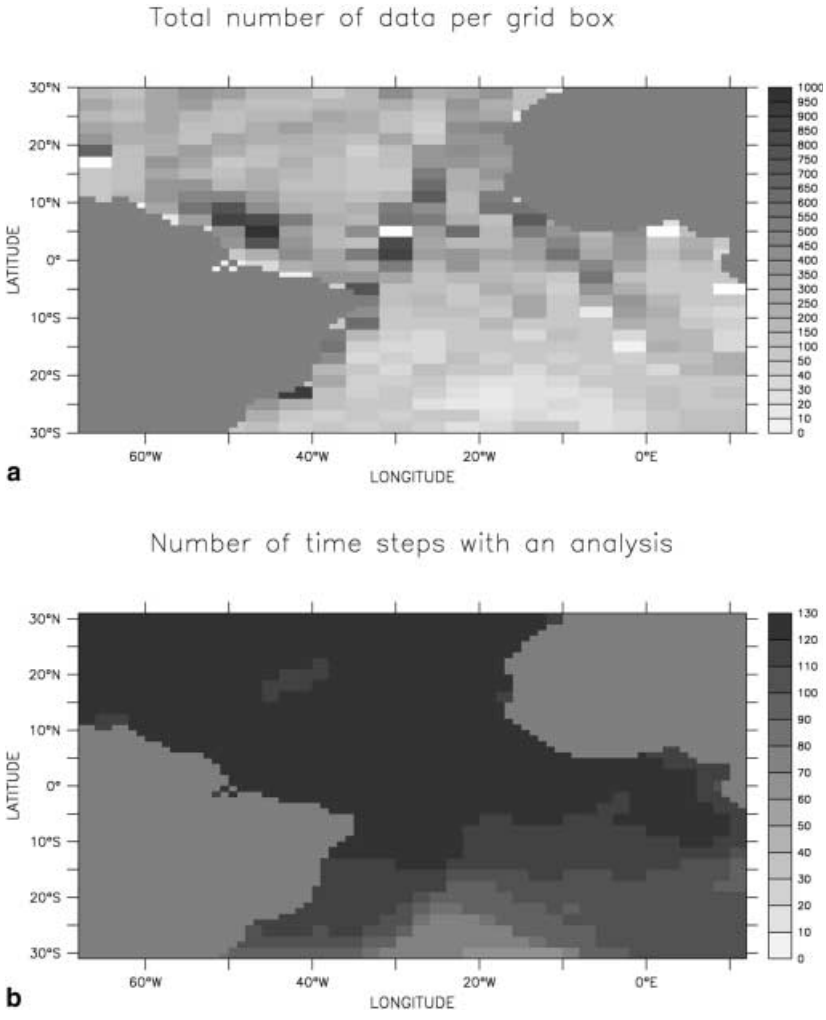

Fig. 2 **a** number of profiles by box (2° × 4°) before objective analysis summed for the 20 years. *White box* means number of data greater than 1000. **b** Number of space-time boxes (2° × 2°× 2 months) filled after analysis. A value of 120 means that the series has been completed at this location

Table 1 Data used for objective analysis

Data type	Data source	Instrumental noise used for objective analyses in percent
XBT	Centre TOGA/WOCE of the SISMER	8
XBT	World Ocean Atlas from Levitus (1994)	8
CTD	World Ocean Atlas from Levitus (1994)	3
CTD	WOCE	2
CTD	Centre TOGA/WOCE of the SISMER	2
CTD	PICOLO campaigns	2
CTD	NOE campaigns	2
Moorings	PIRATA	3
Moorings	CIPREA/FOCAL/SEQUAL	3
Nansen casts	World Ocean Atlas from Levitus (1994)	5
Nansen casts	Russian campaigns	8
CTD	Russian campaigns	8

on XBT data collected between 1967 and 1994, did not correctly represent the annual cycle in a few areas of strong seasonal variability such as in coastal upwellings. In order to eliminate these spurious biases, we computed anomalies for the new seasonal climatology at each grid point. It should be noted at this point that our analysis induces errors due to the constant correlation radius. In fact, in regions of strong mesoscale variability such as coastal upwelling areas, correlation radius are probably smaller than in the open basin, therefore our analysis tends to smooth the coastal upwelling signal too widely.

Figure 2b illustrates the grid coverage in space and time after objective analysis. A box value of 120 means that there is no gap in the time series and that analysis has filled all gaps. This is the case north of 10°S. However, in the southern central part of the basin (between 10°W and 30°W, 20°S and 30°S) the amount of data is not sufficient to fill all time steps in the grid. In this area, about half of the time steps are filled by the analysis. The lack of data is especially significant before 1982. After 1983 the coverage in space and time is more adequate for studying the variability except in 1989 (Fig. 1). Nevertheless it will be necessary to take into account the lack of data in the southern area in the statistical study.

We validate our data base by comparing it with existing products such as SST fields (Reynolds 1993). Correlation coefficients between TAOSTA SST and Reynolds SST are higher than 0.9 and regression coefficients are very close to 1 for practically the whole basin.

A reduction in the correlation coefficient (with a minimum of 0.7) has been observed in areas of strong variability (e.g. upwellings). In these areas, the slope of regression indicates if TAOSTA SSTs are higher or lower than the Reynolds' SSTs. Off Mauritania, slopes of regression are about 1.2, which means that the analysis has underestimated SSTs in this area. On the other hand, below the ITCZ area, slopes are lower than 1 (0.7, 0.8). These biases can be explained by the choice of correlation scales for the objective analysis, which were selected to catch the climatic variability and not small-scale phenomena. As a consequence, small and mesoscales phenomena have been smoothed.

3 Results

We first compare the seasonal cycle with existing climatologies and then study interannual variability while identifying the principal modes. The warming trend of the tropical Atlantic for the 20 last years is also pointed out.

3.1 Seasonal cycle

The seasonal cycle of the tropical Atlantic SST is well known. It has been described in many studies (e.g. Merle et al. 1980), but is not as well documented for subsurface levels. The seasonal cycle is small under the thermocline, with an amplitude less than 0.5 °C at 300 m (figure not shown). At 300-m depth, there is a permanent relatively strong horizontal gradient of temperature between 10°N and 20°N. Two permanent minima are centred on 40°W–7°N and 10°S–15°W.

D20 is representative of the core of the thermocline in the tropical Atlantic and thus is a good indicator of the thickness of the warm upper layer in the tropical Atlantic Ocean. The climatology of the thermocline depth shows two regions of deepest thermocline associated with subtropical gyres, in the northwestern part of the basin, and in the southwest (close to the Brazilian coast) where D20 reaches 200 m in depth. The thermocline depth shows a strong gradient in the across-shore direction in coastal upwelling regions (Mauritania, Angola). In July–August, the cold tongue due to equatorial upwelling is clearly identified by a shallowing of the thermocline along the equator. From July to December, the Guinea dome, associated with a shallowing of the thermocline, is distinguishable and centred on 12°N–22°W as described in Voituriez (1981). Sometimes, D20 is near the surface or even outcrops. The analysis assumes that data are not taken into account when the climatological D20 is less than 10 m in depth (first level of our grid). This is the case in coastal upwelling off Mauritania from March to June and in the southeastern area form July to December.

Figure 3 shows the seasonal cycle of the heat content. The patterns appear to be similar to D20. We found two regions of high heat content which correspond to regions of deep thermocline (centred on 20°N–60°W and 20°S–40°W) associated with the subtropical anticyclonic gyres. Two regions of low heat content are also identified (off the Angolan and Guinean coasts). These areas correspond to the thermal domes as decribed in Voituriez (1981) and Siedler et al. (1992). Thermal domes are typical structures of the eastern tropical oceans where the thermocline is shallow. They are associated with surface cyclonic geostrophic gyre induced by the poleward rotation of the North and South Equatorial Countercurrents (NECC and SECC). Because of the northward tilt of the ITCZ in the east, the Northern Hemisphere dome is better defined than the Southern Hemisphere one (Fig. 3). Voituriez (1981) and Siedler et al. (1992) showed that the subthermocline dome is a permanent, quasi-stationary feature whereas the thermocline dome is more influenced by surface conditions: winds, atmospheric pressure. Thermocline structure is an uplift of subthermocline permanent dome when condition are propitious.

The upper thermal structure of the tropical Atlantic Ocean interacts strongly with the structure of the winds. The NE (northeast) trade winds are strongest in

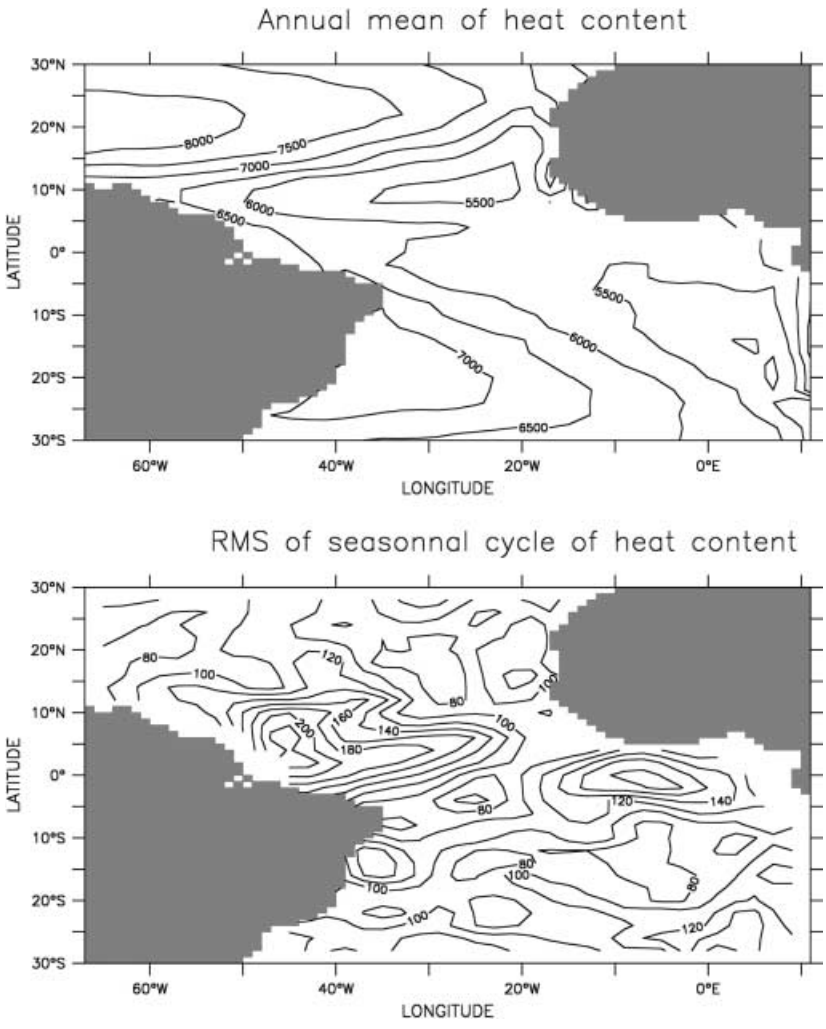

Fig. 3 Climatology of heat content (°C.m). The *top* shows the annual mean and the *bottom* shows the rms of the seasonal cycle

February when the South Atlantic Ocean is warmest and the SE trade winds are strongest in August when the North Atlantic Ocean is warmest. This seasonal oscillation is associated with the meridional excursion of the ITCZ which is close to the equator in February and which reaches sub-Saharan Africa and northern South America along 9°N–10°N in August (Wagner 1996).

3.2 Interannual variability

3.2.1 General characteristics

We first describe some general characteristics of interannual variability over the last 20 years which is apparent from TAOSTA data set. Then, we shall examine four specific events that can be identified as unusual in our analysis. Finally, some simple statistical techniques will be used in order to distinguish the main modes of variability.

On average, a warming trend of the tropical Atlantic basin (30°N–30°S) has become apparent over the last 20 years and especially during the Nineties, of the order of 0.2–0.3 °C at the surface (Fig. 4). This trend is also visible for heat content. The time series for the temperature and heat content averaged over the domain shows that this warming is modulated by interannual variability. Warm events in 1984 and in 1988–1989, for instance, are clearly distinguished. The heat content trend involves subsurface conditions that can explain the observed differences with the SST. The warming trend since 1984 has been more continuous in heat content than in SST which is more affected by atmospheric variability.

In spite of the strong seasonal signal which dominates the tropical Atlantic variability, interannual deviations are significant. The order of magnitude of interannual anomalies (deviations from the mean seasonal cycle) is 2 °C at 10 m in depth and 1.5 °C at 300 m in the Gulf of Guinea (2°W–2°S), 1.5 °C at 10 and 300 m in the northwest area (51°W–12°N), and 1.6 °C at 10 and 300 m in the area straddled by the ITCZ. Thus, below the thermocline, the interannual variability signal is greater than the annual cycle, unlike at the surface.

In order to characterise the areas of maximum variability, root mean squares (rms) have been computed on

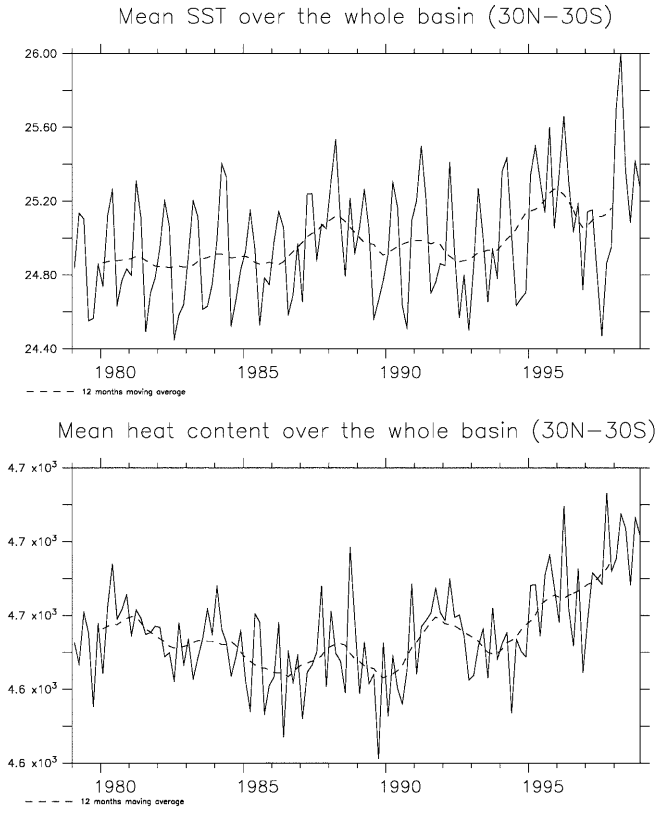

Fig. 4 Mean sea surface temperature (°C) and heat content (°C.m) over the whole tropical Atlantic basin (30°N–30°S). *Dashed lines* are a 12 month moving average

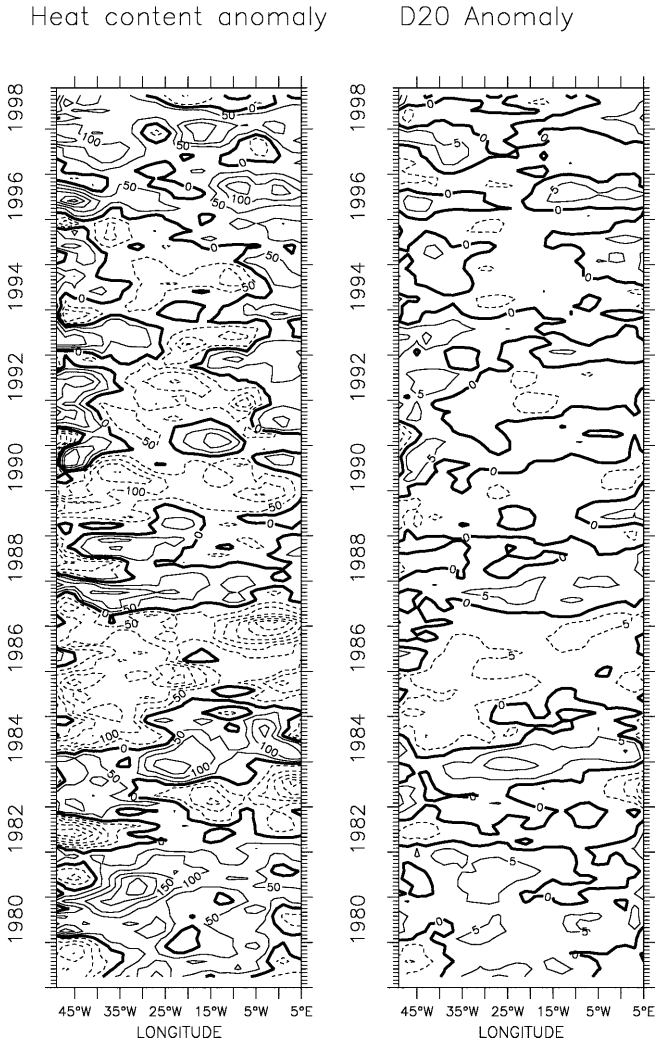

Fig. 5 Hovmuller diagram on the zone 2°S–2°N of heat content (°C.m) and D20 (m) anomaly. Contour intervals are 100 °C.m for heat content and 5 m for D20

SST, heat content and D20 anomalies. Larger rms values are found in the eastern basin and smaller in the western basin. A maximum of rms variability of SST is located in the Gulf of Guinea (0.9 to 1 °C) and in coastal upwelling regions along Mauritania and Angola (1.2 to 1.3 °C). Heat content anomaly rms (not shown) are quite homogeneous between 150 °C.m and 200 °C.m over the basin except in coastal upwellings where rms reaches 350 °C.m. For the D20, the pattern looks different. Areas of maximum variability are in the subtropics (north of 10°N and south of 10°S) where rms reaches about 30 m. Variability in the equatorial regions is weaker (between 3 and 9 m) except in the Gulf of Guinea where it reaches about 20 m.

SST time series along the equator (not shown) reveals a succession of cold and warm events. A warm event is defined following Carton and Huang (1994). We shall consider years in which the SST anomaly in the eastern equatorial region (6°S–2°N, 20°W–10°E) exceeds 0.5 °C for more than one month. In terms of this definition, four characteristic warm events occurred during the last 20 years: 1983–1984, 1987–1990, 1994–1995 and 1997–1998. We shall focus our attention on the period (typically 2 years) around the warm event. Figure 5 illustrates the evolution of the D20 anomalies and of the heat content along the equator. One finds a succession of warm and cold periods on an interannual (few years) time scale. These features indicate clearly that the (0–400 m) heat content variability is directly related to D20 and to the thickness of the warm upper layer as found in Merle et al. (1980) and in Merle (1980). In previous studies, it was not possible to calculate these variables from in-situ data except for relatively short periods (e.g. FOCAL/SEQUAL experiment, Hisard et al. 1986; Reverdin et al. 1991a) and along ship routes. Correlation coefficients between D20 and heat content anomalies (not shown) are high over the whole basin ($r \geq 0.7$), except in the southeast part and in areas of coastal upwellings along Mauritania and Angola. In these areas, D20 is close to the surface and sometimes outcrops. The region where D20 anomaly and heat content anomaly are the most correlated ($r \geq 0.80$) is the northwest part of the basin. This is the area of deepest thermocline associated with maximum heat content.

Figure 6 shows that SST anomaly and D20 anomaly are not strongly correlated ($r = 0.2$ at 95% significance level). In spite of this relatively poor correlation, there is

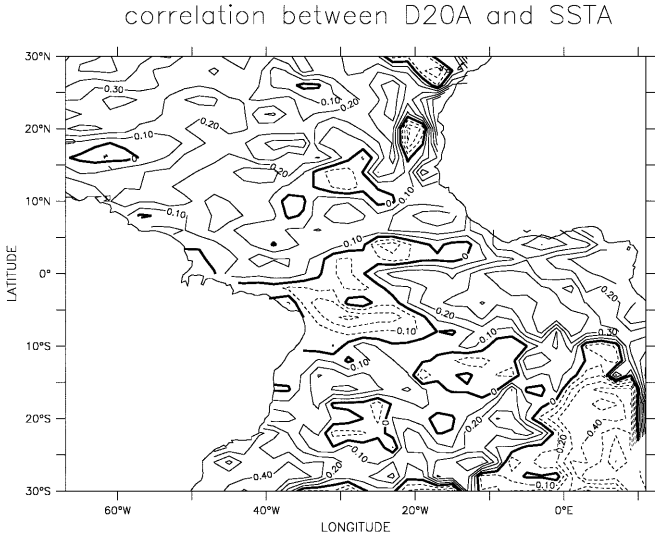

Fig. 6 Correlatiom map between D20 anomaly and SST anomaly from TAOSTA data set. Positive (negative) values are represented by *solid* (*dashed*) lines. The contour interval is 0.1. The significant correlation coefficient at 95% is 0.2

an interesting pattern in the equatorial zone (between 5°N and 5°S). In this area, correlations are predominantly positive in the eastern part of the basin and negative in the western part as found in modelling studies (Servain et al. 2000). This means that in the western part, deepening of the thermocline is associated with cooling of the surface layers whereas in the eastern part, deepening of the thermocline is associated with warming of the surface layers. This can be explained following Carton and Huang (1994). The relaxation of the winds has several effects on the ocean: it induces an inhibition of local upwelling of cold water and reduces zonal advection of cold water westward. Thus the western part warms up in spite of a shallowing of the thermocline.

The area with negative correlation between SST anomalies and D20 anomalies has a narrow band extending to the west along 1°N–3°N. The dynamics of this region are complex and linked to horizontal shearing (Bryan et al. 1995). Except for the equatorial western region, areas with negative correlation are upwelling areas (equatorial and coastal) and the southeastern region where the thermocline is near the surface and sometimes outcrops.

3.2.2 Specific events

Over the period 1979–1999, some characteristic warm events can be identified. Some of them have already been described in studies based on surface conditions or on modelling results (e.g. Carton and Huang 1994). We now consider several specific events that can be identified as unusual in our analysis. In the years 1983–1984, the FOCAL/SEQUAL program collected data in order to study variability in the equatorial Atlantic. These two years showed distinct seasonal cycles (Philander 1986; Zebiak 1993) and some (Hisard et al. 1986) qualified the 1984 event as an "Atlantic El-Niño". In 1983, whereas the tropical Pacific recovered from the significant 1982–1983 El-Niño event, easterlies along the equator strengthened, particularly in May and June 1983 (Fig. 7) associated with an accumulation of warm water in the western part of the basin. In response to the change in the thermocline depth (D20), the heat content increased in the west and decreased in the east. Extreme SST anomalies observed are +1 °C in the west and −2 °C in the east. At the end of November 1983, there was a relaxation of the easterlies along the equator followed by an eastward displacement of the warm anomaly, along the equatorial wave guide. Then, a significant warming in the Gulf of Guinea (0.4 °C–0.8 °C) occurs in March–April 1984. At the same time, the thermocline slope and zonal heat content gradient weakens. Warm SST anomalies were located between 10°W and 30°W at the end of 1984. At the same time, significant rains were recorded in usually arid areas south of the equator in Africa and the coastal upwelling along Angola was reduced (Philander 1986). This phenomenon, initiated by the significant fluctuations of the easterlies at the equator mostly concentrated in the western part, strongly resembles and could have been initiated by the Pacific El-Niño a year earlier (Delecluse et al. 1994). These events have been studied using FOCAL/SEQUAL data set compared to model results by Reverdin et al. (1991b).

The warming mechanism in 1988 looks different. In 1985–1986, the equatorial easterlies were abnormally weak, the thermocline were abnormally shallow (5 m–10 m shallower than normal) and the heat content was abnormally low (Fig. 5). The equatorial region was cooler than normal between July 1986 and March 1987 (Fig. 8) with a maximum of negative anomaly in the Gulf of Guinea (1.5 to 2 °C negative anomalies) in November–December 1986. Then the whole northern basin warmed up rapidly. This warming was observed in SST but not in subsurface variables (D20 and heat content). In January 1988, both NE and SE trade winds became significantly weaker than normal for a season in which equatorial winds normally intensify and induce enhanced Ekman equatorial divergence. This weakening lasted until the end of 1989. It was stronger and lasted much longer than in 1983–1984. As a result, the heat content was abnormally high and the thermocline abnormally deep from June 1987 to March 1988 (Fig. 8) in the equatorial band (5°N–5°S). The thermocline remained deeper than normal (associated with higher than normal heat content) from July 1987 to Autumn 1988. SST remained abnormally high from July 1987 to fall 1989 along the equator. This event involved different mechanisms than the "Atlantic Niño". It had a basin-wide signature in surface variables and an equatorial signature in subsurface variables (D20 and heat content). Significant surface warming in the Gulf of Guinea in October 1987 preceeded the weakening of the

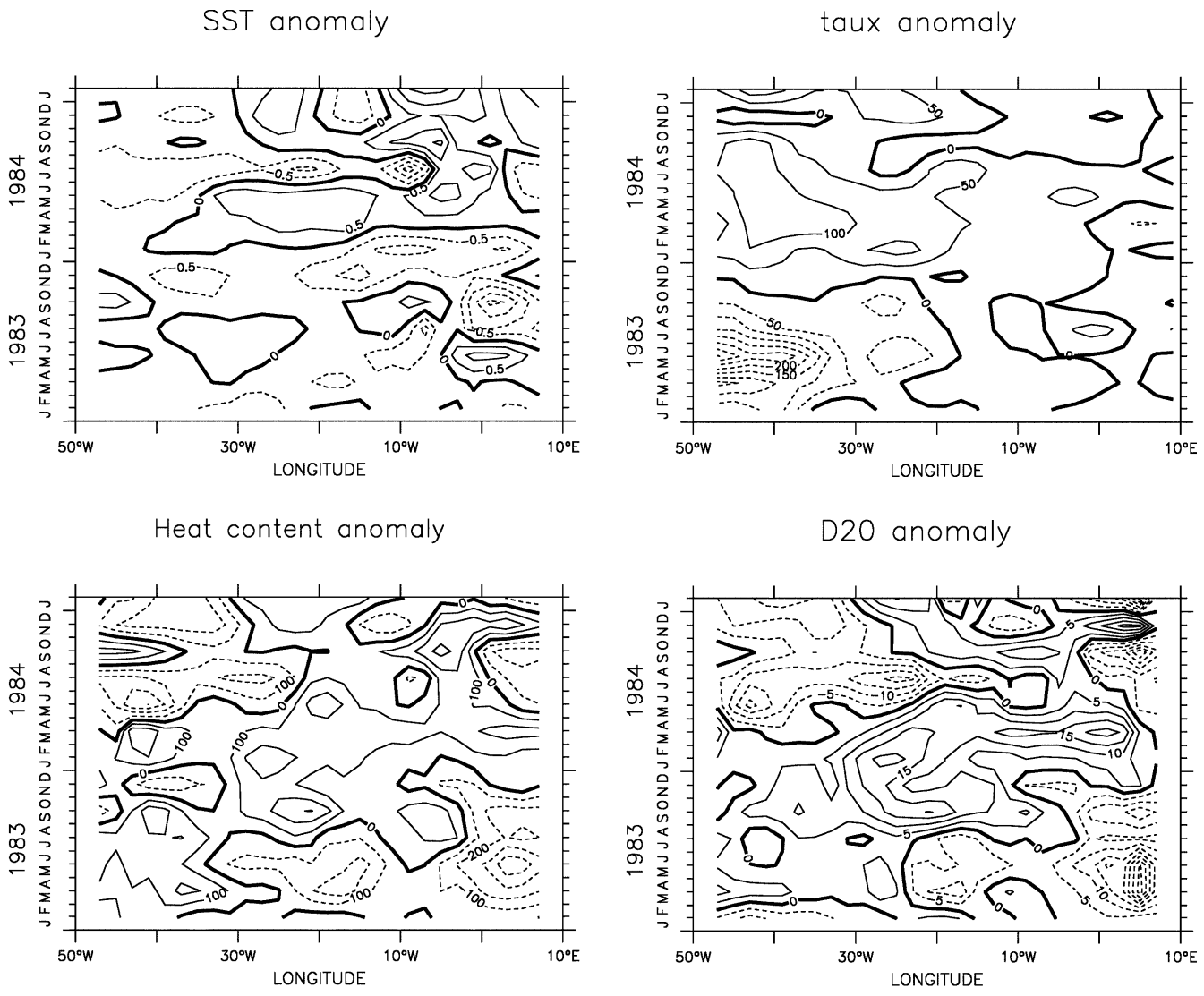

Fig. 7 Hovmuller diagrams for standard TAOSTA variables (SST, heat content and D20 anomalies) and for zonal pseudo wind stress for the 1983–1984 event

equatorial easterlies. The strengthening of the equatorial easterlies in the western equatorial basin was stronger and lasted much longer than the other three events we have described in this section. The northward shift of the ITCZ is associated with a warming in the north, weakening of the NE trade winds, cooling in the south and strengthening of the SE trades. This induced a strengthening of the easterlies in the western equatorial region. Thus, the heat content increased and the thermocline deepened in the west. As the equatorial easterlies weakened in December 1987, the heat content decreased and the thermocline shallowed in the west. This scenario could explain the link between the meridian and equatorial mode as shown in Servain et al. (1998).

In the summer of 1994, the SE trade winds were stronger than normal. They significantly weakened during the winter of 1994–1995 and then returned approximately to the climatological values (figure not shown). The NE trade winds became abnormally strong in winter to spring during 1994 and 1995 inducing enhanced upwelling in Mauritania (2.5 to 3 °C colder than normal in surface layers). Then, they relaxed in May–June 1995 inducing a strong warm SST anomaly between 15°N and 30°N with a maximum reaching 2 °C off Mauritania. This surface warming can be explained by a reduction in heat loss due to the wind weakening. At the same time the SE trade winds returned to their climatological value. Heat content anomalies at the equator then increased continuously and moved eastward reaching maximum anomalies in the Gulf of Guinea in September–October 1995 (Fig. 9). During the warm phase, the zonal gradient of heat content and the zonal thermocline slope decreased. Heat content was abnormally high and the thermocline abnormally deep in the Gulf of Guinea whereas in the western part of the basin, the heat content was abnormally low and thermocline abnormally shallow (anomalies reached 10 m for D20

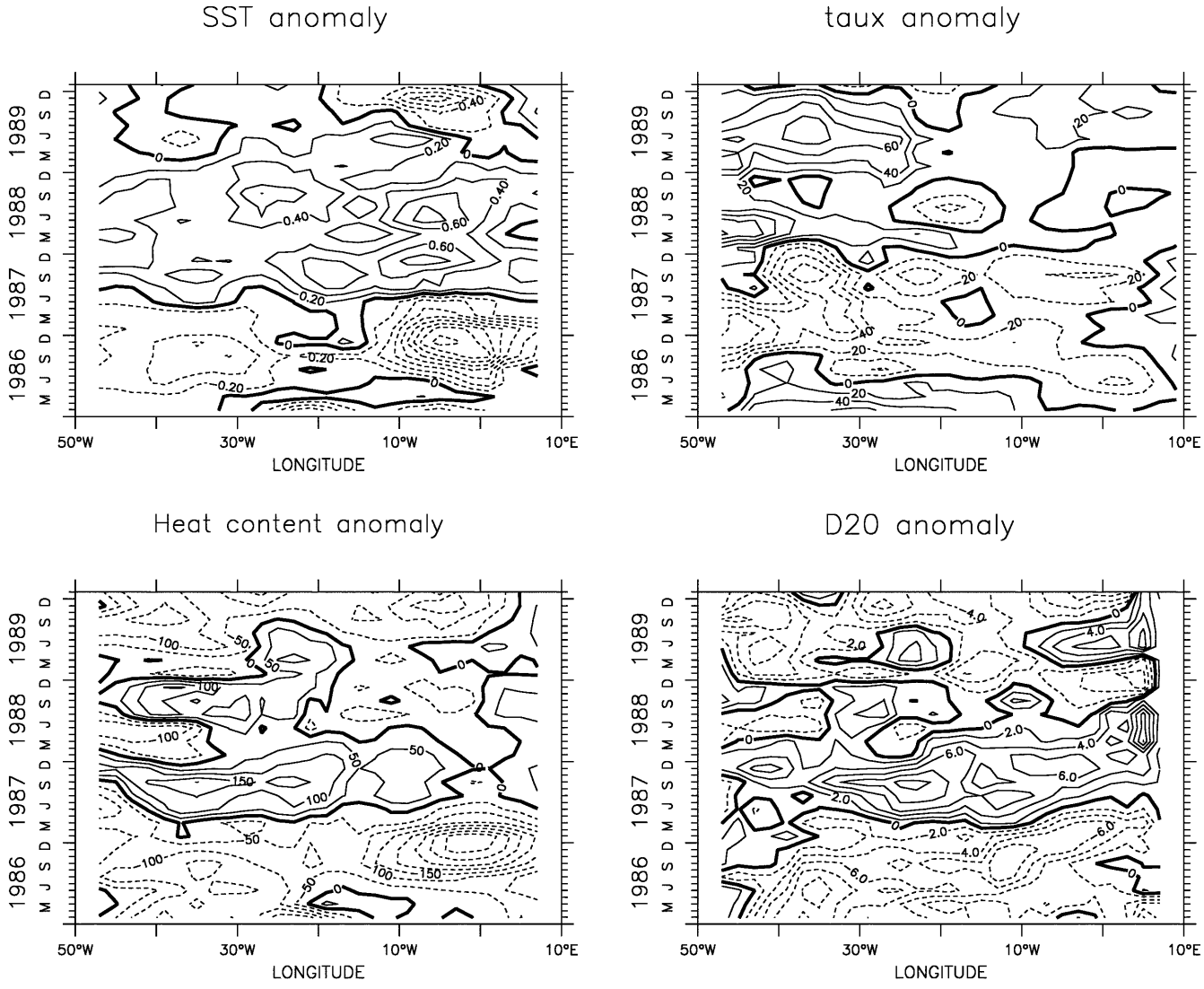

Fig. 8 Same as Fig. 7 for 1988–1989 event

and 150 to 200 °C.m for heat content). Most of the variability associated with this event is confined in the equatoral band (10°N–10°S). The variability of thermocline depth and heat content is characteristic of the "Atlantic Niño" scenario.

The most recent remarkable event occurred in 1997–1998. From February to September 1997, equatorial easterlies were abnormally strong particularly in the western part of the basin and relaxed in September 1997 for a few months (Fig. 10). In summer-fall 1997, as the eastern Pacific warmed up, the SE trade winds were reinforced and extended abnormally far north in the Atlantic. As a consequence, the SST in the Gulf of Guinea was abnormally cold and the heat content in the west was abnormally high associated with an abnormally deep thermocline . During the winter of 1997, the SE trade winds returned to their climatological value whereas the NE trade winds were abnormally weak. SST in the equatorial region and especially in the eastern basin warmed up (+1°) and the Gulf of Guinea remained abnormally warm until April 1998. At the same time, the heat content anomaly increased and the thermocline deepened in the Gulf of Guinea. Maxima of heat content and thermocline anomalies in the east occurred in February–March 1998 corresponding to the highest SST (Fig. 10). Then, equatorial easterlies were again reinforced (Fig. 10) in the west and remained stronger than normal west of 10°W until August 1998. This reinforcement was associated with a deepening of the thermocline and an increase of the heat content west of 20°W (Fig. 10) which reached a maximum in July–August 1998. In the following fall, SST increased along the equator and especially in the east. The second warm event at the end of 1998 was weaker but well marked. The 1997–1998 event presented similar mechanisms to those of the 1983–1984 and 1994–1995 events. However its relation with the Pacific ENSO differs strongly as in 1997–1998, the Pacific El-Niño and the Atlantic events happened almost simultaneously. Thus it is more difficult to conclude that the Pacific El-Niño had initiated the Atlantic phenomenon than for the two other events. Why then did the late 1997 warm event develop

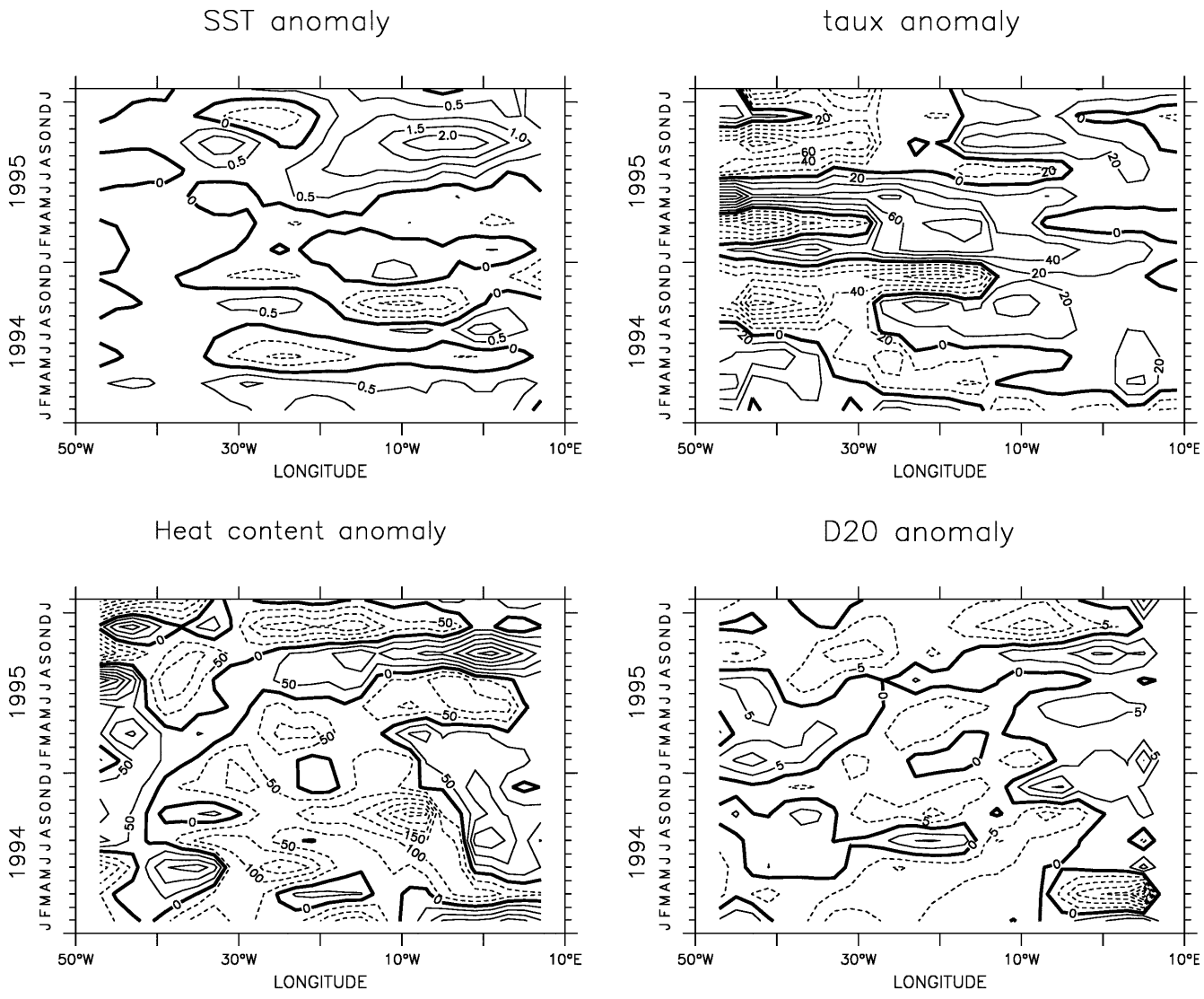

Fig. 9 Same as Fig. 7 for 1994–1995 event

simultaneously in the eastern Pacific and in the eastern Atlantic?

The response of the Atlantic to external forcing seems to be sensitive to the season and particularly to seasonal upwelling at the equator. During the upwelling season (boreal summer), anomalies at the equator develop more easily and are stronger.

3.2.3 Statistical decomposition: EOFs

In order to distinguish the principal modes of variability, we computed a decomposition in empirical orthogonal function (EOFs). We decompose the function $F(x,t) = \sum \alpha_i f_i(x) g_i(t)$ where f_i and g_i are two sets of orthogonal functions in space and time, obtained by diagonalising the covariance matrix. The corresponding eigenvalues represent the portion of the variance corresponding to these structures. This is one way to identify the major modes of space-time variability. The spatial structures and temporal functions have been normalised as follows: each temporal mode has been standardised by its larger module component, thus max $(|v|) = 1$. The associated space mode has been divided by the normalising factor and multiplied by the associated eigenvalue so that the spatial structure indicates the largest value associated with the mode.

We calculated EOF on SST, D20 and heat content anomalies. The first mode is characterised by a meridional contrast between north and south with the region of maximum variance centred in coastal upwelling areas (Mauritania, Angola) (Fig. 11). It expresses a modulation in the meridional gradient of SST anomalies. Its time variability is dominated by a quasi-decadal signal which has been noted over the last 20–30 years in historical observed SSTs (Fontaine et al. 1999). The second mode represents the warming trend over the whole basin. (The associated temporal function closely resembles Fig. 4a). The third mode is equatorial (in phase along the equator but the maximum variance is in the eastern part, centred near coastal upwelling areas). This mode reveals weak

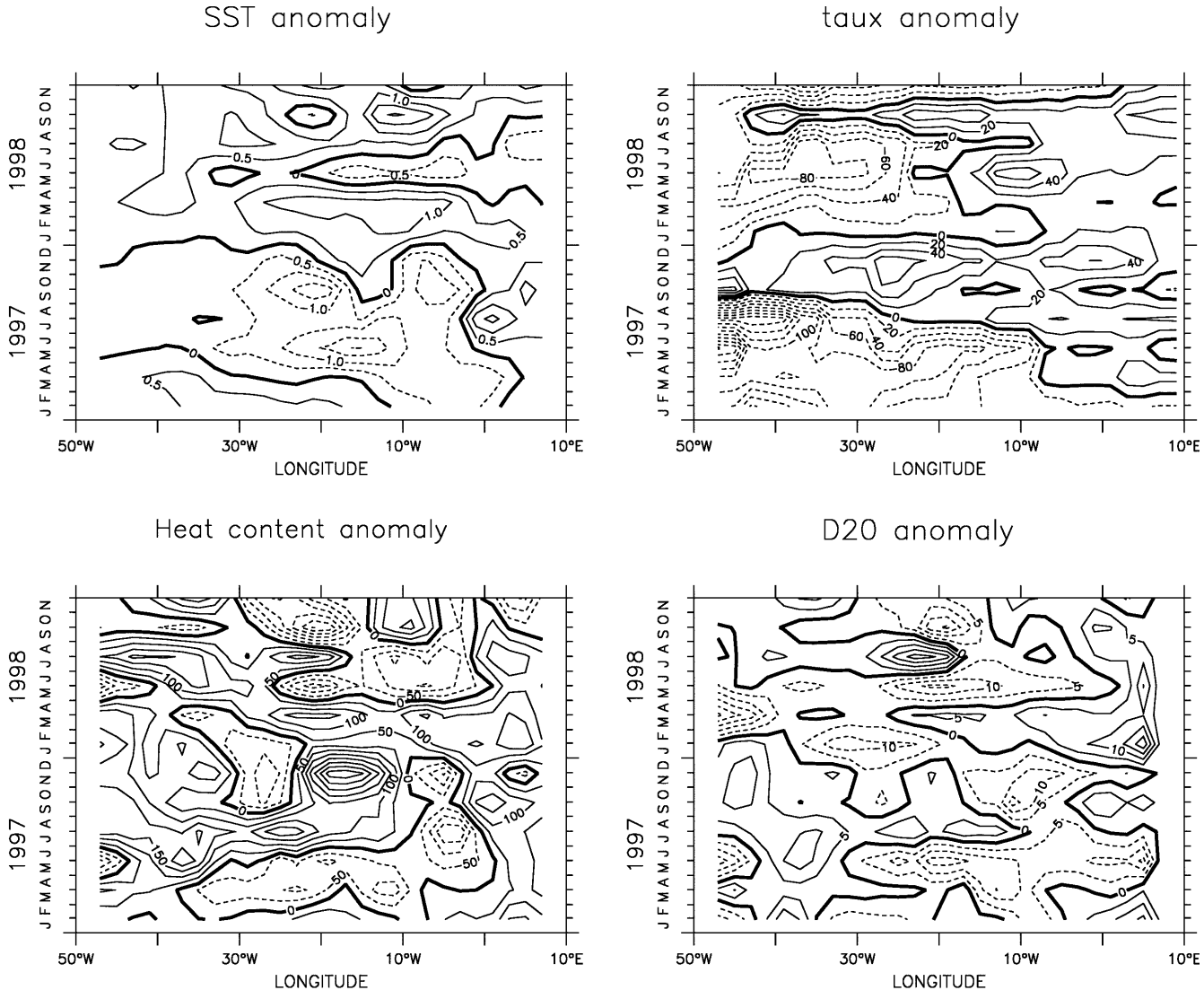

Fig. 10 Same as Fig. 7 for 1997–1998 event

variability in the western part. The temporal function shows a significant multi-annual scale of variability once it has been smoothed with a 12 months running mean. The analysis of SST reveals the same well-known characteristics as in previous studies (e.g. Servain 1986, 1991; Nobre and Shukla 1996 among others).

For the D20 and the heat content, we restricted the study area to 10°S–20°N in order to prevent the subtropical processes from dominating the analysis. The first mode characterises the variability in the northwestern part of the basin (centre on 15°N–55°W) where the thermocline is deepest (Fig. 12). The temporal function reveals a multiannual time scale of variability. The second mode is dominated by a zonal oscillation north of the mean ITCZ position and the third mode shows the zonal equatorial oscillation characteristic of the variability of the thermocline depth in the equatorial region.

Decomposition of the heat content reveals different patterns (Fig. 13). The most energetic mode characterises the trend for the whole basin. It decreases until the end of the 1980s and then increases until the present time. There would appear to be a decadal scale of variability. The second mode is characteristic of the zonal oscillation in the equatorial areas associated with the third mode of D20. The third mode reveals four poles of variability if the Mauritania upwelling is not taken into account. The two western poles (centred on 15°N–60°W and 5°N–40°W) and the two eastern poles (centred on 17°N–30°W and 2°N–0°E) vary in phase and are of the same order of magnitude. It is important to note that this decomposition is very sensitive to the domain of analysis (in space and time). If we reduce the domain to 10°N–10°S, the equatorial mode for D20 and heat content is clearly the most energetic (figure not shown).

Patterns of SST appear to be different to those of D20 and heat content. SST interacts directly with atmospheric variables such as winds and solar radiation, whereas D20 and heat content are linked to ocean dynamics.

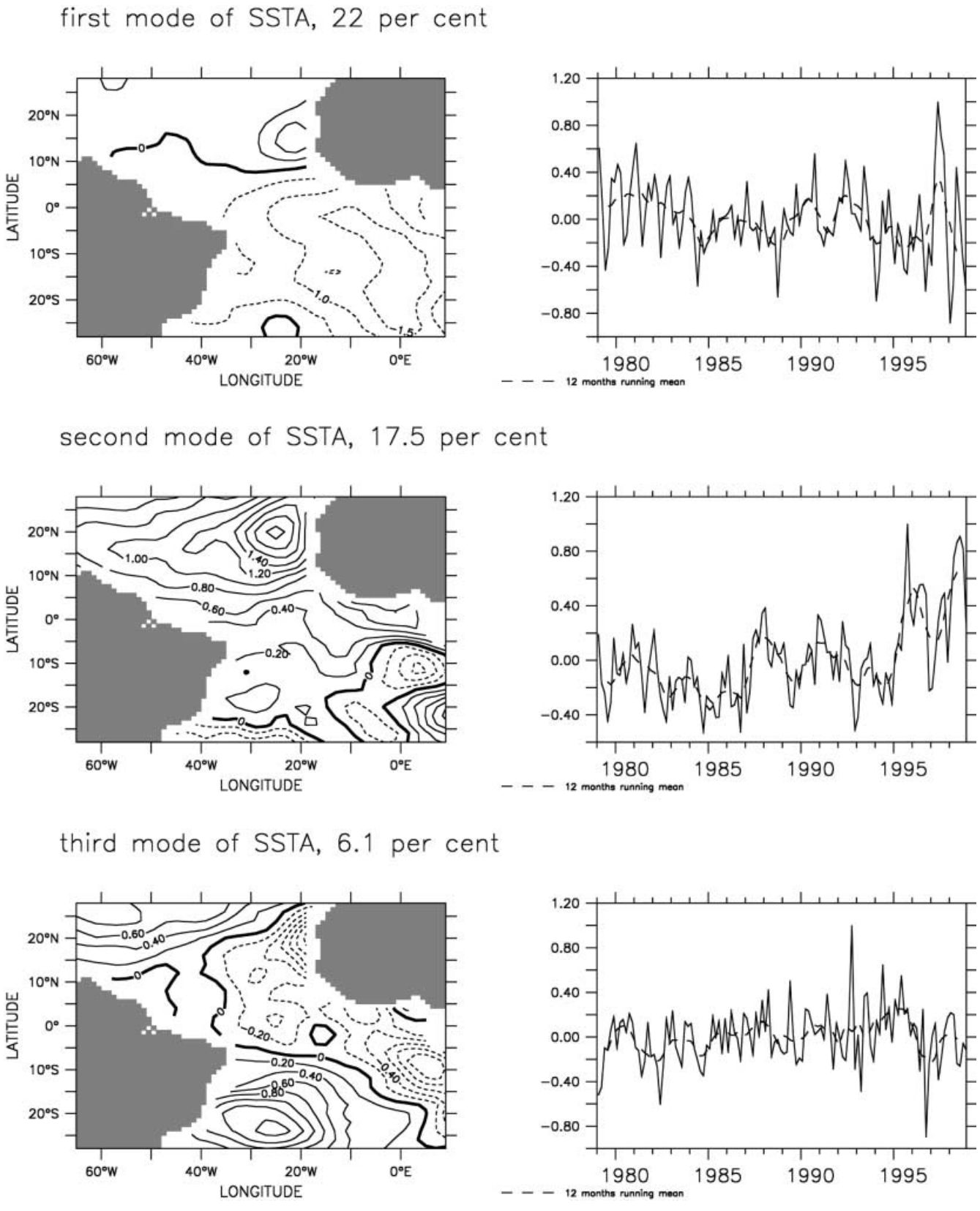

Fig. 11 Three most energetic modes for the sea surface temperature. The *curves* on the *right* panels represent the associated temporal functions, *dashed lines* are a 12 month moving average

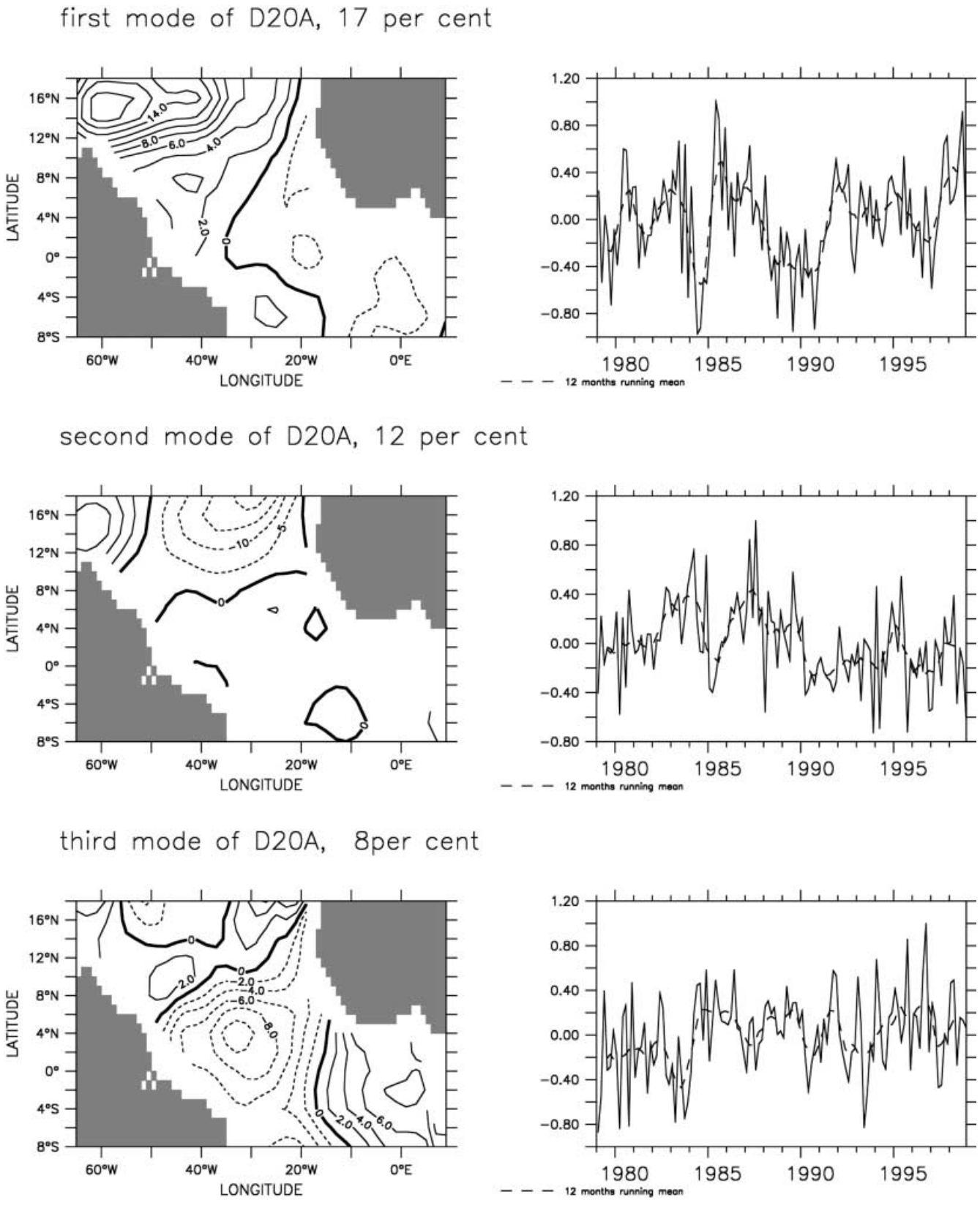

Fig. 12 Most three energetic modes for D20. We have restricted the study area to 10°S–20°N in order not to take into account a subtropical signal which would dominate the analysis. The *curves* on the *right* panels represent the associate temporal functions, the *dashed lines* are a 12 month moving average

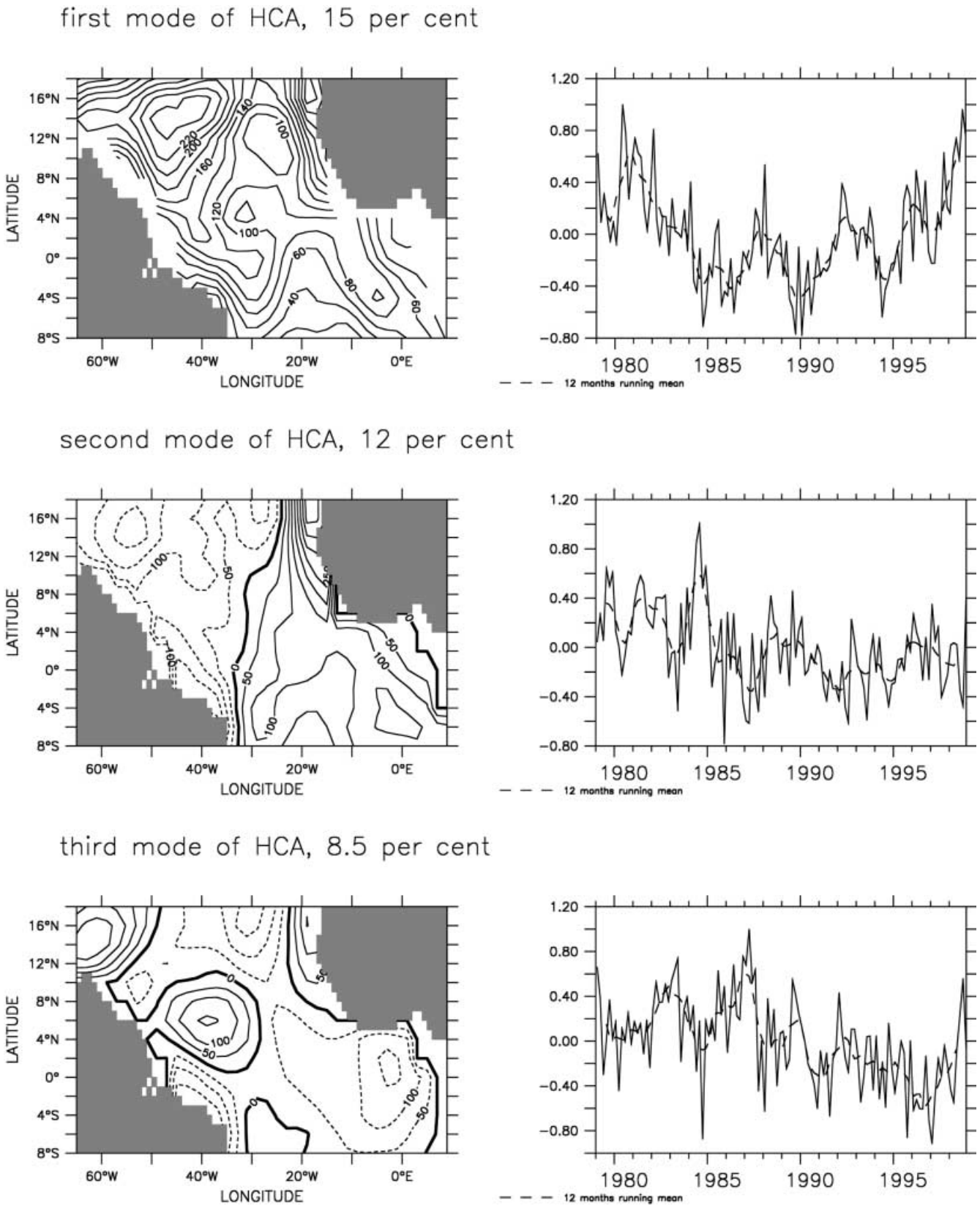

Fig. 13 Same as Fig. 12 for heat content

3.3 Correlation with climatic indices

In this section, we investigate the impact of the equatorial Pacific and North Atlantic Ocean on tropical Atlantic variability. Climatic characteristic indices (NINO3, SOI, NAO, and a zonal wind index) are used. The zonal wind index has been chosen for the western equatorial Atlantic (30°W–35°W, 2°N–2°S) in order to study the response of the tropical Atlantic to the variability of the western equatorial easterlies. (We calculated cross correlation between climatic indices and TAOSTA variables with temporal lag from 2 to 12 months, the climatic index being in advance in relation to TAOSTA variables).

3.3.1 Pacific influence

We computed lagged cross-correlation and regression between the SOI index (normalised pressure difference between Tahiti and Darwin) and TAOSTA standard variables (SST, D20 and heat content anomalies) and between NINO3 index (mean Pacific SST between 150°W–90°W and 5°N–5°S) and TAOSTA standard variables (SST, D20 and heat content anomalies). We choose to show our results with NINO3, since correlations are more significant with similar patterns. Pacific Ocean variability affects Atlantic ocean through atmospheric disturbances (Delecluse et al. 1994). Some discussions about possible links can be found in a few diagnostic studies (Horel et al. 1986, Enfield and Mayer 1997) and in atmospheric modelling studies (Mechoso et al. 1990).

Influence on SST

At lag 0 (not shown), a dipolar structure appears, characterised by a positive correlation north of the mean ITCZ region and negative south of it. The maximum correlation is found when tropical SST variability lags behind the NINO3 index by four months (Fig. 14) when the area of negative correlation is confined to a tongue between the average position of the ITCZ and 10°S. The critical correlation coefficient at 95% level of significance is 0.2. The maximum of positive correlation (warming) is in the northwestern part of the domain (this is consistent with results described in Enfield and Mayer 1997). The maximum of negative correlation (cooling) is situated in the east, south of the equator (centred on 5°S). At lag 6 (not shown) an equatorial structure appears (warming in the Gulf of Guinea and cooling in the western part of the basin). This pattern is reinforced until lag 10 (Fig. 14). Calculation of the regression slopes indicates that a unit of NINO3 index (1 °C of SST) leads to a negative anomaly from 0.25 to 0.3 °C for areas of maximum correlation. Strong El-Niño (3 °C anomalies in the Eastern Pacific) can thus induce anomalies of about 1 °C in significant zones of the Atlantic (Gulf of Guinea, northwestern tropical Atlantic). As found by Enfield and Mayer (1997) SST anomalies in tropical Atlantic are correlated with ENSO in several regions. The major area with the strongest correlation is the North Atlantic area of NE trade winds west of 40°W along 10°N–20°N and extending into the Caribbean. Enfield and Mayer (1997) found that 50 to 80% of the SSTA variability in that region is associated with ENSO with a lag of four–five months. In our study, we found the same area of correlation with a maximum correlation at four months. This warming in the northwestern area can be explained as follows: the warm phase in the eastern Pacific induces a reduction in the surface NE trade wind speed, hence a reduction in latent and sensible heat losses as well as a cooling due to entrainment over that region. The second region of significant covariability with ENSO is the equatorial band. The intensification of the easterlies in the western equatorial part appears to be associated with northward migration of the ITCZ when North Atlantic warming occurs. Warming in the northwestern part of the basin following the mature phase of El-Niño induces a northward shift of the ITCZ. The easterlies thus intensify in the western equatorial zone preceding by a few months cooling in the eastern equatorial region, and warming in the western equatorial region.

Influence on D20

Until lag 4, there is a significant positive correlation between D20 and the NINO3 index which corresponds to a deepening (or shallowing) of the thermocline in the western (respectively eastern) part of the basin (Fig. 14). From lag 6, the deepening in the equatorial area extends gradually towards the east whereas the deepening of the northwestern region is reduced and moves southwards along the South American coastline. Regression coefficients indicates the order of magnitude of D20 anomalies corresponding to a unit of NINO3. Thus, at lag 4, a strong El-Niño can involve a deepening (or shallowing) of 15 m in the west (or in the east). In a model study, Delecluse et al. (1994) found that the wind signal anomalies in the tropical Atlantic are partly induced by eastern Pacific SST anomalies. This AGCM (atmospheric general circulation model) captured well the strengthening of the trade winds over the equatorial Atlantic during 1983 and the subsequent weakening of the trade winds at the begining of 1984. In the spring of 1984, the deepening of the thermocline in the eastern equatorial Atlantic was also simulated in the ocean model. Delecluse et al. (1994) showed that the tropical Atlantic equatorial mode (''Atlantic El-Niño'') partly resulted from ENSO with a 1 year lag. Our results are coherent with those of Delecluse et al. (1994).

Influence on heat content

Not surprisingly, the correlation pattern between the NINO3 index and the heat content anomalies reveals a similar structure. Figure 14 shows correlation coefficients at lag 4 and lag 10. A deepening of thermocline corresponds to an increase in heat content and vice versa. This suggests that during a significant El-Niño event, surface warming occurs north of the average position of the ITCZ with a lag of one to four months. This

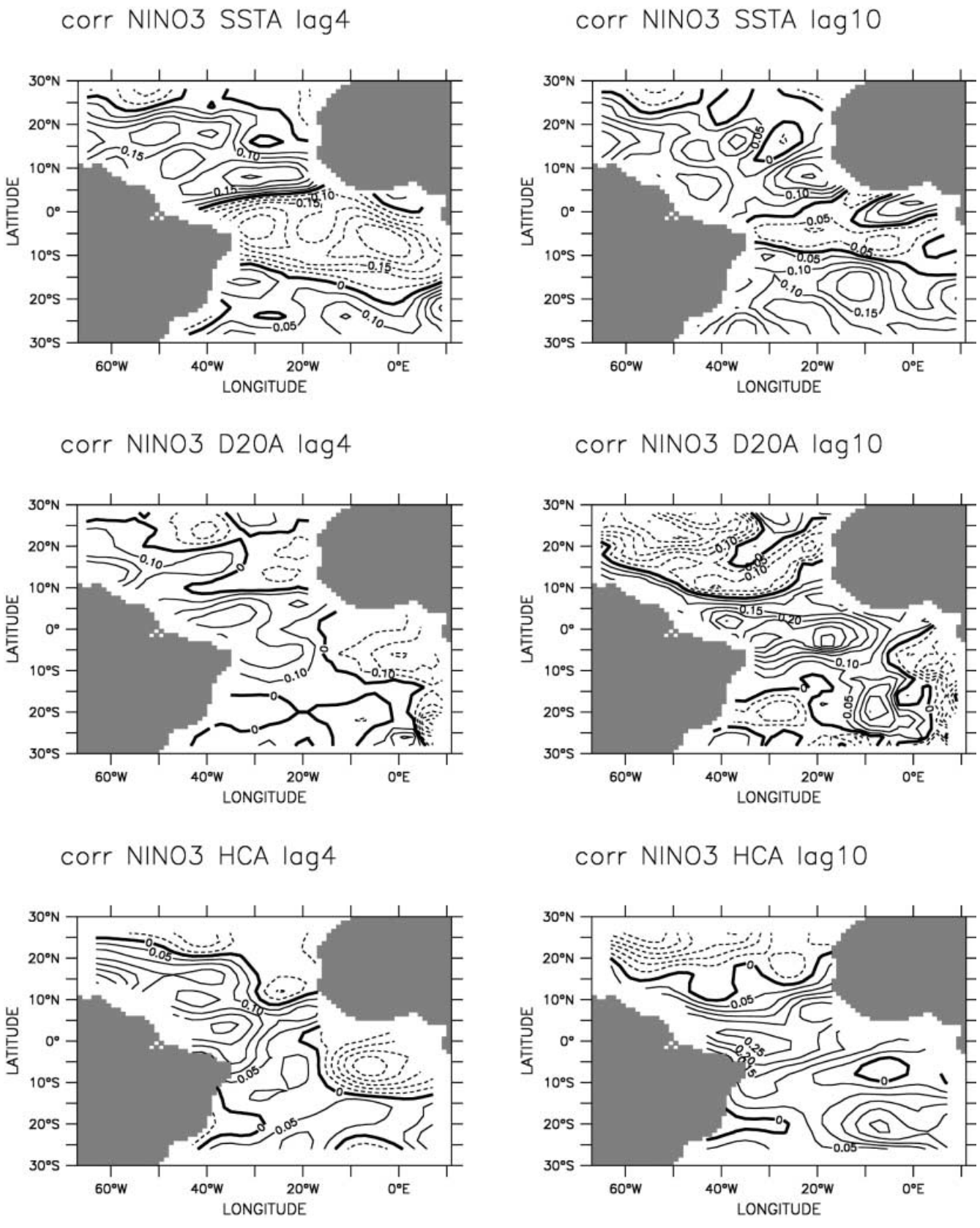

Fig. 14 Correlation between the NINO3 SST index and standard TAOSTA variables (SST, D20 and heat content anomalies). The critical correlation coefficient at a 95% significance level is 0.2

is linked to thermocline deepening and an increase in heat content. In the eastern part, the D20 shallows and the heat content decreases with a maximum correlation slightly south of the equator (as on SST pattern). Then, the thermocline slope relaxes (shallowing in the west and deepening in the east) and the zonal heat content gradient vanishes (decreasing in the west and increasing in the east) as the Gulf of Guinea warms up. An equatorial structure appears at the surface (warming of the Gulf of Guinea and cooling in the west associated with eastward displacement of deep thermocline and high heat content). Ten to twelve months after the mature phase of El-Niño, one would thus have a signal in the tropical Atlantic which would appear to correspond to the "Atlantic El-Niño".

3.3.2 North Atlantic influence

The correlation between NAO winter index and SST anomalies is marginally significant ($r = 0.25$) in a band between 10°N and 20°N. A high NAO (stronger low pressure over Iceland and stronger high pressure over the Azores) is associated with abnormally strong NE trade winds that induce cooling of the surface. The correlation is more significant (Fig. 15) if we only take winter SST anomalies (January 30). A high NAO winter index is associated with cooling of the surface in the NE trade region and especially between 5°N and 15°N in the central basin, and with a significant warming in the northwestern part of the basin. A high NAO winter index is associated with a southward displacement of the trade wind system. Thus, NE trade winds are reinforced and winds in the northwestern part weakened.

The correlation between the NAO winter index and heat content of winter is marginally significant (figure not shown). The only region in which the correlation coefficient is higher than 0.3 is the NE trade wind region where a high NAO winter index is associated with an abnormally low heat content. A high NAO winter index is associated with abnormally strong NE trade winds, hence we find cooling of the surface due to enhanced heat losses, and deepening of mixed layer depth inducing abnormally low heat content.

3.3.3 Zonal wind influences

The tropical ocean responds very quickly to a change in wind stress. We investigated how the tropical Atlantic reacts under the influence of zonal wind variability in the western equatorial part. A zonal wind index is defined as the zonal component of the pseudo-stress (from Servain et al. 1996) averaged over the area 30°W to 35°W and 2°N to 2°S. We choose this area to estimate the variability of the easterlies as it seems to initiate the equatorial mode. Interannual anomalies are estimated using the seasonal cycle corresponding to the period of study (1979 to 1998). The zonal component of the trade wind is negative westward, thus a positive anomaly of index means weaker easterlies. We calculate regression and correlation coefficients between this zonal wind index and TAOSTA standard variables for lags up to 1 year (the wind index is in advance in relation to the TAOSTA variables). Correlations are highest at lag 4 (Fig. 17).

At lag 0, the only region where correlation between the zonal wind index and TAOSTA standard variables is significant with a 95% level of significance (the critical correlation coefficient is 0.2) is the North Atlantic area of NE trade winds along 15°–20°N west of 35°W (Fig. 16). This warming can be explained by the reduction of latent and sensible heat losses and cooling due to entrainment resulting from the weakening of the trade winds in that region a few months after a Pacific El-Niño event (Enfield and Mayer 1997). At lag 2 we find a significant signal (at 95% level of significance) corresponding to a cooling in the northwest (centred on

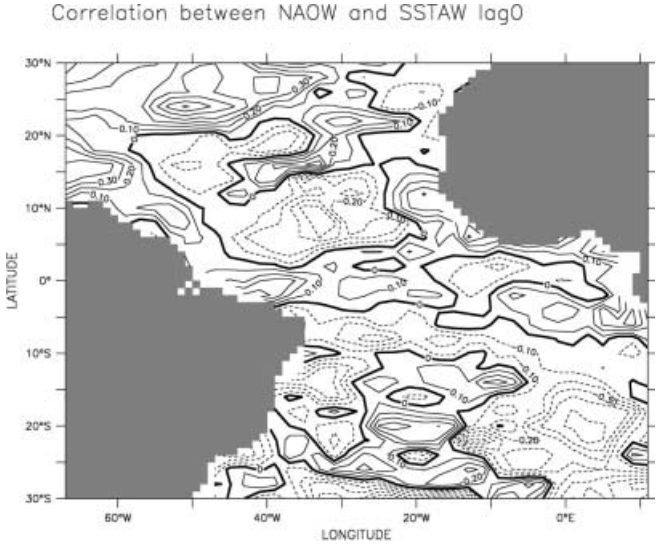

Fig. 15 Correlation between NAO winter and SST anomalies from TAOSTA data set (winter: January 30)

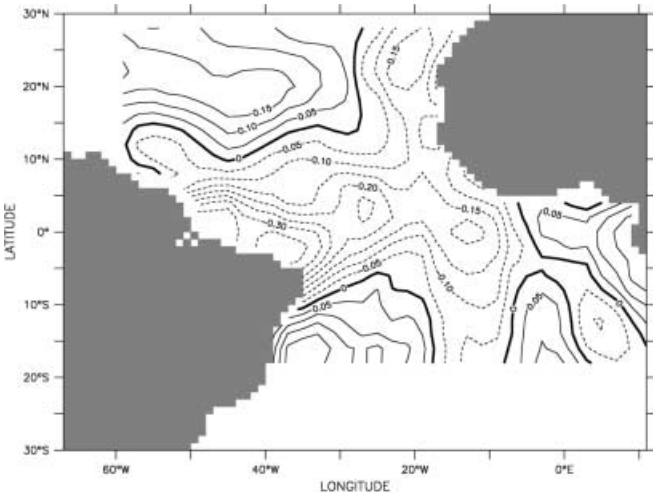

Fig. 16 Correlation at lag 0 between NINO3 SST index and zonal wind anomaly

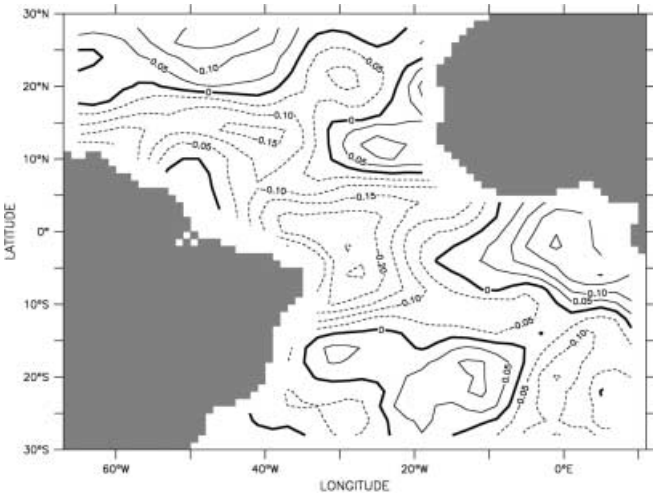

Fig. 17 Correlation at lag 4 between zonal wind index and thermocline depth anomalies

15°N–50°W) and to a warming of the equatorial region (5°N–15°S). This warming accentuates and the maximum of correlation gradually moves eastwards with increasing time lags. It reaches a maximum at lag 6 ($r \geq 0.4$) in a zone centred on 5°S–3°W. Then, at lag 8, the maximum of correlation gradually spreads southward and back into the interior of the basin (figures not shown) as shown by Carton and Huang (1994) in a study based on 28 years of SST record. The warming area extends from the coast of South America to 3°W. At lag 12, correlations are not significant apart from a positive correlation ($r \geq 0.3$) in a region centred on 25°N–50°W.

Correlations are significant at lag 4 and lag 6 where an equatorial mode is well marked . There is an equatorial pivot centred on 15°W (Fig. 17) first shown by Merle et al. (1980). In the west, correlations are negative (deepening of the thermocline) and in the east, they are positive (shallowing of the thermocline). Thus, 4 to 6 months after strengthening of the equatorial easterlies, thermocline slope and zonal heat content gradient are at a maximum.

The phenomenon described for D20 is also identifiable for the heat content in spite of weaker, but nevertheless significant correlation. When a significant relaxation of the easterlies occurs close to the equator, four months later, the region between the mean ITCZ position and 15°S warms up with maximum correlation in the eastern part, centred near 5°S. This is associated with a relaxation of the thermocline slope and zonal heat content gradient (with a maximum correlation at lag 4). At lag 8, correlations are no longer significant. The phenomenon observed here is connected with and strongly resembles the Pacific El-Niño. The mature phase of the ''Atlantic Niño'' would occur approximately 4 to 6 months after a significant relaxation of the trade winds and one year after its Pacific counterpart.

This study suggests an impact of the Pacific equatorial variability on the Atlantic through atmospheric disturbances. Using simple statistical techniques, we found that Atlantic warm events usually lag behind Pacific El-Niño events by 1 year as suggested in modelling studies by Delecluse et al. (1994). A significant Pacific El-Niño induces a strengthening of the trade winds in the equatorial Atlantic region and a weakening of the easterlies in the northwestern region (Fig. 16). This structure persists until lag 4 when the thermocline slope and zonal heat content gradient are highest. From lag 6, correlations between easterlies and the NINO3 index are no longer significant, the trade winds weaken, the thermocline slope and zonal heat content gradient vanishes. Lags 10 to 12 correspond to the mature warm phase in the Atlantic (''Atlantic Niño'').

4 Discussion

Specific warm events in the equatorial Atlantic have been identified in the SST anomalies in the eastern equatorial basin. They are associated with heat content and thermocline depth anomalies. The statistical decomposition (EOFs) of the fields, which identify the principal modes of variability, suggests similarities as well as differences in the three noteworthy equatorial events (1984, 1995 and 1997). These three events seem to have been initiated by zonal wind variabilities and are thus an oceanic response to equatorial winds, which in return can affect the atmosphere. They are characterised by surface warming associated with an increase in heat content and thermocline deepening in the eastern part of the basin. The mature phase of these three events lasted for a few months. Analysis showed that the surface and subsurface variables are linked. These events were confined in an equatorial band (5°N–5°S) and clearly involved subsurface dynamics. The main difference between the three is related to the period of weakening of the easterlies in the western basin following the period of strong easterlies. During the 1983–1984 event, trade winds were abnormally strong from March to October 1983 inducing enhanced equatorial upwelling which brought cold water to the surface. During the 1994–1995 event, strong trade winds occurred from September to December 1994. During 1997–1998, a period of abnormally strong equatorial easterlies lasted from fall 1996 to September 1997 and the weakening occurred in September 1997. Equatorial easterlies remained abnormally weak until January 1998, followed by a second period of strong equatorial easterlies which occurred from February 1998 to August 1998. The 1988 event would appear to be different, as the variability of the equatorial easterlies did not initiate the phenomenon. In fact, the surface warming associated with heat content increase and thermocline deepening began in June–July 1987 whereas equatorial easterlies weakened in January 1988. We can thus distinguish two patterns associated with the principal modes of variability. One, confined to the equatorial band, is clearly initiated by the variability of the western

equatorial winds and strongly involved subsurface equatorial dynamics through equatorial waves adjustment, the second is a basin-wide mode which is not initiated by the equatorial winds variability and is not so clearly linked to subsurface equatorial dynamics.

The relationship between Pacific Ocean variability, characterised by SOI and the NINO3 index, and Atlantic Ocean warm events has been investigated in many studies (Covey and Hastenrath 1978; Hastenrath et al. 1987; Wolter 1989, among others). Some modelling studies have also established evidence of links between tropical Atlantic trade wind variability and the ENSO phenomenon (Carton and Huang 1994; Delecluse et al. 1994).

Our study reinforced this idea of the significant influence of ENSO as a partial explanation of the tropical Atlantic Ocean variability. As El-Niño matures in the Pacific (high NINO3 index and low SOI index), south-easterly trade winds strengthen, north-easterly trade winds weaken and the ITCZ shift northward. The meridional position of the ITCZ has a great influence on rainfall variability over the African Sahel (Tanaka et al. 1975) and in the Nordeste region of Brazil (Ward and Folland 1991). The anomalous northward shift of the ITCZ, which can be associated with a Pacific El-Niño event, induces a reduction in heat losses between 10°N and 20°N as found in Curtis and Hastenrath (1995) and thus the observed SST warming (Chang et al. 1997), D20 deepening and heat content increase in that region. Simultaneously, the intensification of the SE trade winds induces cooling in the southern part of the basin (0°–15°S). At the equator, SST is abnormally cool, especially in the east, associated with tropospheric subsidence and hydrostatic adjustment of the atmosphere (Covey and Hastenrath 1978; Lindzen and Nigam 1987).

Four months after NINO3 peaks, the Atlantic easterlies at the equator relax inducing a relaxation in thermocline slope and a zonal heat content gradient. Ten to twelve months after a Pacific El-Niño event and 4 to 6 months after the weakening of the equatorial easterlies, the thermocline flattens at the equator, the zonal heat content gradient vanishes and the Gulf of Guinea warms up. These mechanisms might involve coupled dynamics that are not yet clearly understood. Atlantic warm events statistically occur approximately 1 year after Pacific El-Niño events but each event is different.

The interannual variability of the tropical Atlantic is more complex than that of the tropical Pacific. Several modes of variability interact and some are not confined to the tropics. The well-known SST modes are pointed out (''interhemispheric mode of gradient'' and equatorial mode). For subsurface variables (D20 and heat content), variability in the northern part of the basin dominates the first mode. The third EOF in D20 and the second EOF in heat content reveal the equatorial modes. However results of the statistical decomposition are sensitive to the domain of study.

The tropical Atlantic basin variability is strongly influenced by the surrounding continents: the geographical position of South America and West Africa induce an asymmetry in climatic patterns of variability that are therefore more complex than those observed in the Pacific. These will have to be investigated further and will require a much expanded observational network and modelling effort.

Acknowledgements We would like to thank Robert Molinari for providing his XBT climatology, and Pierre De Mey for initiating us in the NADA OI code. The authors are grateful to Gilles Reverdin for making useful suggestions and comments.

References

Bretherton FP, Davis RE, Fandry CB (1976) A technique for objective analysis and design oceanographic experiments applied to mode-73. Deep Sea 23: 559–582

Bryan FO, Wainer I, Holland WR (1995) Sensitivity of the tropical Atlantic circulation to specilication of wind stress climatology. J Geophys Res 24: 729–744

Carton J, Huang B (1994) Warm events in the tropical Atlantic. J Phys Oceanogr 24: 888–903

Chang P, Ji L, Li H (1997) A decadal climate variation in the tropical Atlantic Ocean from thermodynamic air-sea interactions. Nature 385: 516–518

Covey D, Hastenrath S (1978) The Pacific El Niño phenomenon and the Atlantic circulation. Mon Weather Rev 106: 1280–1287

Curtis S, Hastenrath S (1995) Forcing of anomalous sea surface temperature evolution in the tropical Atlantic during Pacific warm events. J Geophys Res 100: 15 835–15 847

De-Mey P, Benkiran M (2000) A multivariate reduced-order optimal interpolation method and its application to the Mediterranean basin-scale circulation. In: Pinardi N (ed) Ocean forecasting, conceptual basis and applications. Springer, Berlin Heidelberg New York (in press)

Delecluse P, Servain J, Levy C, Bengston L (1994) On the connection between the 1984 Atlantic warm event and the 1982–1983 ENSO. Tellus 46A: 448–464

Enfield DB, Mayer A (1997) Tropical Atlantic sea surface temperature variability and its relation to El-Niño-Southern Oscillation. J Geophys Res 102: 929–945

Fontaine B, Janicot S, Roucou P (1999) Coupled ocean-atmosphere surface variability and its climate impacts in the tropical Atlantic region. Clim Dyn 15: 451–473

Gustavsson N (1981) A review of methods for objectives analysis. In: Bengtsson L, Ghil M, Kallen E (eds) Dynamic meteorology – data methods. Springer New York, pp 330

Hastenrath S, Castro LC, Aceituno P (1987) The southern oscillation in the tropical Atlantic sector. Contrib Atmos Phys 60: 447–463

Hisard P, Henin C, Houghton R, Piton B, Rual P (1986) Oceanic conditions in the tropical Atlantic during 1983 and 1984. Nature 322: 243–245

Horel JD, Kousky VE, Kagano MT (1986) Atmospheric conditions in the Atlantic sector during 1983 and 1984. Nature 322: 248–251

Houghton RW, Tourre YM (1992) Characteristics of low-frequency sea surface temperature fluctuations in the tropical Atlantic. J Clim 5: 765–771

Lindzen RS, Nigam S (1987) On the role of sea surface temperature gradients in forcing low level winds and convergence in the tropics. J Atmos Sci 44: 2440–2458

Lorenc AC (1986) Analysis methods for numerical weather prediction. Q J R Meteorol Soc 112: 1177–1194

Mayer DA, Molinari RL, Festa JF (1998) The mean and annual cycle of upper layer temperatures field in relation to Sverdrup dynamics within the gyres the Atlantic Ocean. J Geophys Res 103: 18 545–18 566

Mechoso CR, Lyons SW, Spahr JA (1990) The impact of sea surface temperature anomalies on the rainfall over northeast Brazil. J Clim 3: 812–826

Mehta VM, Delworth T (1995) Decadal variability of the tropical atlantic ocean surface temperature in shipboard measurement and in a global ocean-atmosphere model. J Clim 8: 172–190

Merle J (1980) Variabilité thermique annuelle et interannuelle de l'océan atlantique équatorial est, l'hypothese d'un "el niño" atlantique. Oceanol Acta 3: 209–220

Merle J, Fieux M, Hisard P (1980) Annual signal and interannual anomalies of sea surface temperature in the eastern equatorial Atlantic. Deep Sea Res 26: 77–101

Moura AD, Shukla J (1981) On the dynamics of drought in northeast brazil: observation, theory and numerical experiments with a general circulation model. J Atmos Sci 38: 2653–2675

Nobre P, Shukla J (1996) Variations of sea surface temperature, wind stress, and rainfall over the tropical Atlantic and South America. J Clim 9: 2464–2479

Philander SGH (1986) Unusual conditions in the tropical Atlantic Ocean in 1984. Nature 322: 236–238

Reverdin G, Delecluse P, Levy C, Andrich P, Morliere A, Verstraete JM (1991a) The near surface tropical Atlantic in 1982–1983: results from a numerical simulation and a data analysis. Prog Oceanogr 27: 273–340

Reverdin G, Rual P, du Penhoat Y, Gouriou Y (1991b) Vertical structure of the seasonal cycle in the central equatorial Atlantic ocean: XBT sections from 1980 to 1988. J Phys Oceanogr 21: 277–291

Reynolds RW (1993) Improved global surface temperature analyses using optimum interpolation. J Clim 2: 114–119

Servain J (1986) Empirical orthogonal function analyses of tropical Atlantic sea surface temperature and wind stress: 1964–1979. J Geophys Res 91: 14 181–14 191

Servain J (1991) Simple climatic indices for the tropical Atlantic Ocean and some applications. J Geophys Res 96: 15 137–15 146

Servain J, Stricherz JN, Legler DM (1996) Toga pseudo-stress atlas 1985–1994, vol 1: tropical Atlantic. Edité par Centre Orstom de Brest

Servain J, Wainer I, Dessier A (1998) Evidence d''une liaison entre les deux principaux modes de variabilite climatique interannuelle de l''atlantique tropical. Acad Sci Paris 327: 1–8

Servain J, Wainer I, Ayina HL, Roquet H (2000) A numerical study of relationship between the climatic variability in the tropical Atlantic. Int J Climat (in press)

Servain J, Wainer I, McCreary JP, Dessier A (1999) Relationship between the equatorial and meridional modes of climatic variability in the tropical Atlantic. Geo Res Lett 26: 485–488

Shaeffer JD (1995) Tropical cyclone activity as a diagnostic climate indicator. 20th Annual Climate Diagnostics Workshop Seattle pp 113–116

Siedler G, Zangenberg N, Onken R (1992) Seasonal changes in the tropical Atlantic circulation: observation and simulation of the Guinea dome. J Geophys Res 97: 703–715

Tanaka M, Weare BW, Navato AR, Newell RE (1975) Recent African rainfall pattern. Nature 255: 201–203

Voituriez B (1981) Les sous-courants équatoriaux nord et sud et la formation des dômes thermiques tropicaux. Oceanol Acta 4: 497–506

Wagner RG (1996) Mechanisms controlling variability of the interhemispheric sea surface temperature gradient in the tropical Atlantic. J Clim 9: 2010–2019

Wagner RG, da Silva A (1994) Surface conditions associated with anomalous rainfall in the Guinea region. Int J Climatol 14: 179–199

Ward NM, Folland CK (1991) Prediction of seasonal rainfall in the north nordeste of Brazil using eigenvectors of sea surface temperature. Int J Climatol 11: 711–743

Wolter K (1989) Modes of tropical circulation, southern oscillation and Sahel rainfall anomalies. J Clim 2: 149–172

Zebiak SE (1993) Air-sea interaction in the equatorial Atlantic region. J Clim 6: 1567–1586